Journal of Controlled Release 348 (2022) 938–950

Contents lists available at ScienceDirect

Journal of Controlled Release

journal homepage: www.elsevier.com/locate/jconrel

Modulating albumin-mediated transport of peptide-drug conjugates for antigen-specific Treg induction

Chun Yin Jerry Lau [a,1], Naomi Benne [b], Bo Lou [a,c], Olga Zharkova [c,d], Hui Jun Ting [c,d], Daniëlle ter Braake [b], Nicky van Kronenburg [a], Marcel H. Fens [a], Femke Broere [b], Wim E. Hennink [a], Jiong-Wei Wang [c,d,e,f,*], Enrico Mastrobattista [a,*]

[a] Utrecht Institute for Pharmaceutical Sciences, Department of Pharmaceutics, Faculty of Science, Utrecht University, Universiteitsweg 99, 3584 CG Utrecht, the Netherlands
[b] Department of Infectious Diseases and Immunology, Faculty of Veterinary Medicine, Utrecht University, Yalelaan 1, 3584 CL Utrecht, the Netherlands
[c] Department of Surgery, Yong Loo Lin School of Medicine, National University of Singapore, 1E Kent Ridge Road, NUHS Tower Block, 119228 Singapore, Singapore
[d] Cardiovascular Research Institute, Yong Loo Lin School of Medicine, National University of Singapore, 14 Medical Drive, 117599, Singapore
[e] Department of Physiology, National University of Singapore, 2 Medical Drive, 117593 Singapore, Singapore
[f] Nanomedicine Translational Research Programme, Centre for NanoMedicine, Yong Loo Lin School of Medicine, National University of Singapore, 30 Medical Drive, 117609 Singapore, Singapore

ARTICLE INFO

Keywords:
Peptide-drug conjugates
Albumin transport
Supramolecular medicine
Drug delivery
Antigen-specific tolerance

ABSTRACT

The therapeutic potential of antigen-specific regulatory T cells (Treg) has been extensively explored, leading to the development of several tolerogenic vaccines. Dexamethasone-antigen conjugates represent a prominent class of tolerogenic vaccines that enable coordinated delivery of antigen and dexamethasone to target immune cells. The importance of nonspecific albumin association towards the biodistribution of antigen-adjuvant conjugates has gained increasing attention, by which hydrophobic and electrostatic interactions govern the association capacity. Using an ensemble of computational and experimental techniques, we evaluate the impact of charged residues adjacent to the drug conjugation site in dexamethasone-antigen conjugates (Dex-K/E4-OVA323, K: lysine, E: glutamate) towards their albumin association capacity and induction of antigen-specific Treg. We find that Dex-K4-OVA323 possesses a higher albumin association capacity than Dex-E4-OVA323, leading to enhanced liver distribution and antigen-presenting cell uptake. Furthermore, using an OVA323-specific adoptive-transfer mouse model, we show that Dex-K4-OVA323 selectively upregulated OVA323-specific Treg cells, whereas Dex-E4-OVA323 exerted no significant effect on Treg cells. Our findings serve as a guide to optimize the functionality of dexamethasone-antigen conjugate amid switching vaccine epitope sequences. Moreover, our study demonstrates that moderating the residues adjacent to the conjugation sites can serve as an engineering approach for future peptide-drug conjugate development.

1. Introduction

The therapeutic potential of antigen-specific regulatory T cells (Treg, $CD4^+CD25^+Foxp3^+$) in mitigating autoimmune disorders has been extensively explored [1–3]. The induction of antigen-specific Treg plays a crucial role in alleviating pathological autoimmunity in diseases, such as atherosclerosis [4,5] and Type I Diabetes [2,6]. Tolerogenic vaccines are under development for de novo induction of antigen-specific Treg, in which induction generally requires coordinated delivery of disease-associated antigen and tolerogenic adjuvants (e.g., dexamethasone, an immunosuppressive drug) to the antigen-presenting cells (APCs) [7–10]. In particular, conjugation of an antigen epitope to a tolerogenic adjuvant as a peptide-drug conjugate is a convenient and effective approach to enable coordinated cargo delivery to the APCs (e.g., macrophages, dendritic cells), thereby avoiding the side effects experienced by their stochastic distribution in the body, e.g., off-target immune activation, nonspecific immunosuppression [8,9]. However, due to the relatively small size of the antigen-adjuvant conjugate monomers (< 5 nm), they

* Corresponding author.
E-mail addresses: surwang@nus.edu.sg (J.-W. Wang), e.mastrobattista@uu.nl (E. Mastrobattista).
[1] Current address: Department of Materials Engineering, Graduate School of Engineering, The University of Tokyo, 7-3-1 Hongo, Bunkyo-ku, 113-8656, Japan

https://doi.org/10.1016/j.jconrel.2022.06.025
Received 16 March 2022; Received in revised form 22 May 2022; Accepted 15 June 2022
Available online 29 June 2022

can partially bypass lymphatic transport upon subcutaneous (s.c.) administration via direct blood capillary drainage [11,12], followed by rapid renal clearance [13,14]. Therefore, a physiological transport mechanism is required to deliver them to the biologically active sites (e.g., lymph nodes [15–17], liver [18,19]).

Albumin is the most abundant plasma protein present in different body compartments (e.g., lymphatic, interstitial fluid, blood). It is a major transporter protein for endogenous (e.g., testosterone) and exogenous molecules (e.g., dexamethasone) via transient association [20–22]. Though multiple binding sites are resolved to study specific molecule association to albumin [15,23,24], there is an increasing awareness of the importance of nonspecific albumin association of therapeutic cargos towards their pharmacokinetic and pharmacodynamic properties, in which albumin serves as a reservoir for drug deposition until it is saturated [25–27]. Therefore, there is a need to understand the parameters governing therapeutic cargos' nonspecific albumin association capacity. Furthermore, by playing a crucial role in regulating the colloid osmotic pressure in the body, albumin constantly shuffles between the lymphatic system and the blood capillaries [28]. Albumin also actively mediates liver uptake of the associated molecules [29,30], thereby facilitating the execution of biological activities (e.g., hepatic metabolism [30,31]). Exploiting these transport mechanisms, several drug delivery systems were designed to enhance their target site accumulations [32–34], such as hepatic [35,36] and lymphatic [15–17,35,37] retentions (Fig. 1a). For example, Chen et al. designed a series of peptide-drug conjugates that associate with albumin upon s.c. injection. The albumin/conjugate complexation can enhance the hepatic and lymphatic accumulation of the conjugates, which are essential for eliciting robust antigen-specific immune responses [35]. Irvine et al. have studied a library of peptide conjugates to reveal potential generality of this albumin transport mechanism, in which, despite having different hydrophobic moieties, all peptide conjugates exhibit a certain extent of enhanced lymphatic and hepatic accumulation [16,37]. Nevertheless, most of these studies emphasized optimizing the specific albumin association of peptide-drug conjugates [15–17,35,36]. The parameters governing the nonspecific albumin associations have yet to be systematically explored.

Dexamethasone, a tolerogenic glucocorticoid, is transported primarily via albumin upon systemic administration [38,39]. Albumin has a high capacity for nonspecific dexamethasone association via hydrophobic interactions [39,40]. Even though dexamethasone [23] and testosterone [21] are shown to share the same specific albumin binding site, the level of serum albumin association of dexamethasone at usual dosage is unaffected by the co-presence of testosterone [38]. Furthermore, albumin is also a scavenger protein for charged molecules, e.g., cationic peptides [41,42] and anionic drugs [31]. Since albumin displays a net negative charge at physiological conditions [20], the charge of the molecules (i.e., cationic or anionic) might influence the albumin association capacity. In this regard, it is common for vaccine epitopes to have charged residues flanking at either end of the peptide sequences [43–47]. Since both the N- and C-terminus of peptide sequences are frequently employed for drug conjugation (e.g., carboxylic ester linker [48–50]), the adjacent charged residues might influence how the dexamethasone-antigen conjugates interact with albumin.

The present study explores the impact of switching charged residues adjacent to the drug conjugation site in dexamethasone-antigen conjugates towards the albumin association capacity and induction of antigen-specific tolerance. To this end, four residues repeat of either cationic lysine (K) or anionic glutamate (E) were placed between dexamethasone succinate and model ovalbumin (OVA) major histocompatibility complex (MHC) class II peptide epitope (OVA323: ISQAVHAAHAEINEAGR) to simulate vaccine epitopes flanked with

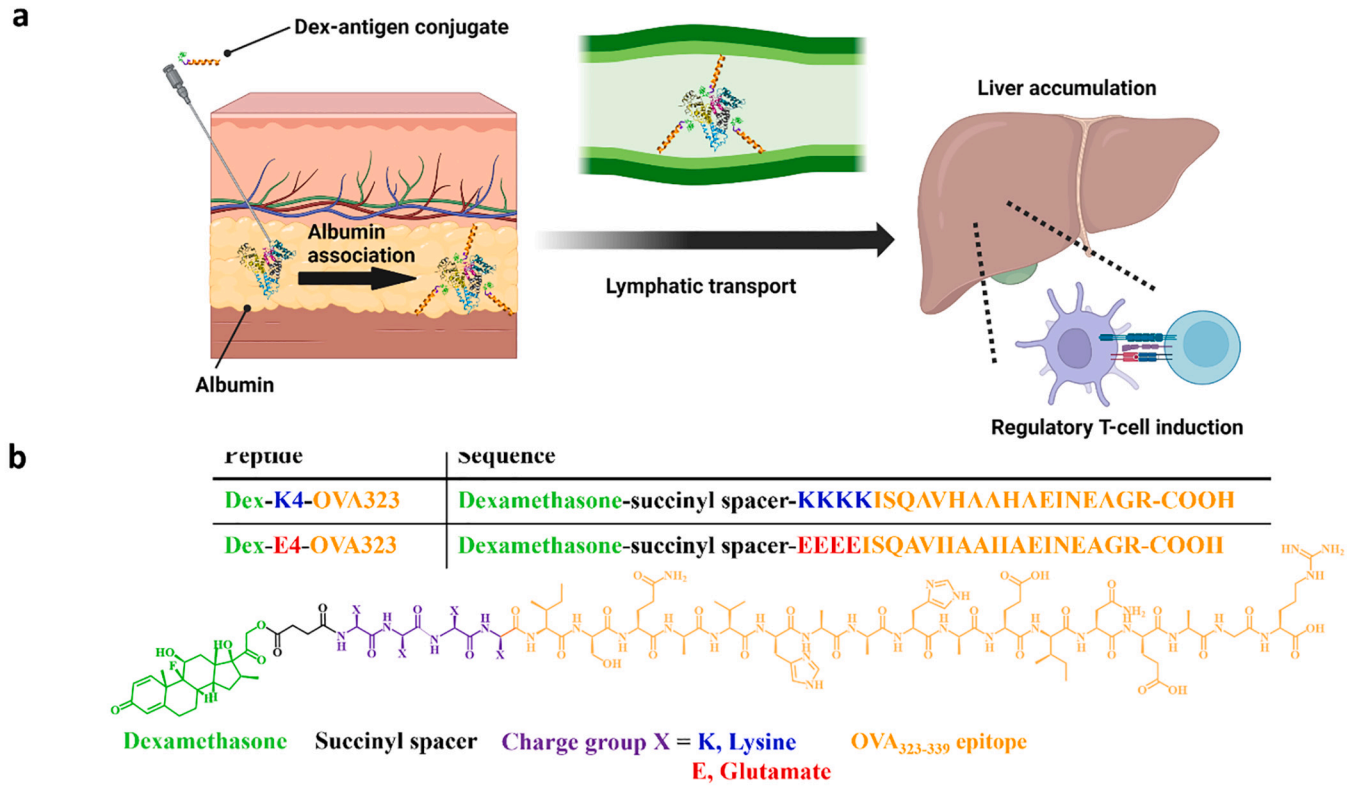

Fig. 1. Working mechanism and molecular details of the dexamethasone-antigen conjugates used in this study. (a) Illustration of the proposed working mechanism of albumin association enhanced tolerogenic immunotherapy. Upon subcutaneous (s.c.) administration, the dexamethasone-antigen conjugates are associated with albumin. Consequently, the complexes are transported to draining lymph nodes and the liver via the lymphatic system, from which the conjugates are taken up by antigen-presenting cells (macrophages and dendritic cells). (b) Chemical structures of the dexamethasone-antigen conjugates. Dexamethasone was conjugated to the peptide sequences via a biodegradable succinyl linker. The N-terminus of the OVA323 epitope sequence was extended with four charged residues (K:+ve or E:-ve).

cationic or anionic residues at the N-terminus. Using coarse-grained molecular dynamics (CG-MD) simulations, we showed that charged residues next to the drug conjugation sites are crucial in mediating their surface association to albumin. Thereby, the albumin association capacity of Dex-K/E4-OVA323 was evaluated through surface hydrophobicity and electrostatic potential analysis, which was subsequently validated with native polyacrylamide gel electrophoresis (PAGE). The lymphatic and hepatic retention of s.c. administered Dex-K/E4-OVA323 was subsequently analyzed. The organ distribution and APCs uptake level were correlated to the antigen-specific tolerance elicited in an OVA323-specific adoptive transfer mice model.

2. Materials and methods

2.1. Materials

Pre-loaded Fmoc-Arg(Pbf)-Wang resin, Fmoc-protected amino acids were purchased from Novabiochem (Darmstadt, Germany). Oxyma pure was obtained from Manchester Organics (Manchester, UK). N, N′-diisopropylcarbodiimide, and acetonitrile (MeCN) were obtained from Biosolve BV (Valkenswaard, the Netherlands). Trifluoroacetic acid, triisopropylsilane, formic acid, ammonium bicarbonate were purchased from Sigma-Aldrich (Zwijndrecht, the Netherlands). Dulbecco's phosphate-buffered saline buffer (1 × PBS, 2.7 mM KCl, 1.5 mM KH_2PO_4, 138 mM NaCl, 8 mM Na_2HPO_4, pH 7.4).

2.2. Synthesis of dexamethasone-antigen conjugates

The peptides were synthesized with standard Fmoc solid-phase chemistry using a Liberty blue peptide synthesizer (CEM Corporation). In brief, for each coupling cycle, 5 eq Fmoc-protected amino acids were activated with 5 eq of Oxyma pure and N,N′-Diisopropylcarbodiimide to react with the free N-terminal exposed on resin for 1 min at 90 °C. After each amino acid coupling, the Fmoc group was deprotected by treatment with 20% piperidine for 1 min at 90 °C. The dexamethasone succinate derivate was prepared as described previously [48]. This compound was subsequently coupled to the side chain protected sequence on resin using the same solid-phase chemistry as other Fmoc-amino acids (Fig. S1). The dexamethasone-antigen conjugate was cleaved with cocktail trifluoroacetic acid/water/triisopropylsilane (95/2.5/2.5) for 2 h at room temperature and purified by preparative reverse-phase HPLC using a Reprosil-Pur 120 C18-AQ column (10um, 250 × 25 mm). The purity and yield of the immunoconjugates were confirmed to be >90% by analytical HPLC using a Waters XBridge C18 column (5 μm, 4.6 × 150 mm), and Mass Spectrometry (MS) analysis was performed using a Bruker microTOF-Q instrument (Note S1–3).

2.3. LigParGen parameterization

The chemical structure of dexamethasone succinate was downloaded from PubChem (CID: 90479300) and optimized with Avogadro software. The structurally optimized dexamethasone succinate MOL file was uploaded to the LigParGen web server for atomic coordinate parametrization [51]. The parameterized dexamethasone succinate was used as an artificial amino acid for further analysis.

2.4. RoseTTAFold and PEP-FOLD3 protein/peptide structure prediction

The de novo protein structure prediction of mouse serum albumin (UniProtID: Q546G4–1) was performed using RoseTTAFold [52]. The predicted lDDT was performed using DeepAccNet [53] to provide a quality score of the model confidence. The best model with <2 Å per-residue error was used for further computational analysis (i.e., albumin 26–608, Fig. S2b). The de novo secondary structure prediction of the K/E4-OVA323 sequences was performed using the PEP-FOLD3.0 server [54,55]. Standard free modeling parameters were chosen for the sequence modeling. The best models were chosen for further analysis. The structural alphabet prediction profile was generated for representing the conformation propensities per residue in the output sequences (Fig. S2c-d).

2.5. CG-MD simulation

The CG models of mouse serum albumin and K/E4-OVA323 were derived from their respective RoseTTAFold or PEP-FOLD3 models using martinize2. An elastic network [56] was applied to maintain the overall structure of albumin, in which the non-bonded interactions between the backbone beads connected by the elastic network were preserved [57]. Dexamethasone succinate was assigned with Martini 3.0 beads [58] according to its chemical properties (Fig. S6). The bonded terms of the dexamethasone succinate CG model were optimized with Swarm-CG software [59] to reach the best agreement with the atomistic model obtained from LigParGen (Fig. S7). The optimized dexamethasone succinate CG model was conjugated to K/E4-OVA323 using polyply software [60] to generate structures and input parameters of Dex-K/E4-OVA323 for the CG-MD simulations.

All CG-MD simulations were performed with GROMACS 2019.6 [61] and Martini 3.0 force field [58]. One albumin and one dexamethasone-antigen conjugate were randomly placed in a 16 × 16 × 16 nm^3 cubic box, in which water and 150 mM NaCl (including neutralizing counterions) were eventually added. The systems were energy minimized with the steepest descent algorithm (50,000 steps), followed by a brief NPT equilibration cycle to relax the initial configurations (100,000 steps of 5 fs). Afterward, the systems were simulated for 2 μs in an NPT ensemble with periodic boundary conditions (100,000,000 steps of 20 fs). The temperature was maintained at 300 K ($\tau_T = 1.0$ ps) and pressure at 1 bar ($\tau_p = 4$ ps) by coupling the dynamics using V-rescale thermostat [62] and Berendsen barostat [63]. The cut-off value for the Coulomb and van der Waals interactions was set to 1.1 nm, and a relative dielectric constant was set to 15.

2.6. Steered MD (SMD) simulations

All SMD simulations were performed with GROMACS 2019.6 [61] and Martini 3.0 force field [58]. The equilibrated structures (2 μs) from the CG-MD simulations were transferred to larger rectangular boxes (13 × 13 × 26 nm^3), in which water and 150 mM NaCl (including neutralizing counterions) were eventually added. The systems were energy minimized with the steepest descent algorithm (50,000 steps), followed by a brief NPT equilibration cycle to relax the initial configurations (100,000 steps of 5 fs). Afterward, a pulling potential (force constant of 1000 kJ mol^{-1} nm^2) was attached to the center-of-mass of dexamethasone-antigen conjugate to dragged them from albumin along z-coordinate in a rate of 0.01 nm ps^{-1}. The albumin was constrained by applying a harmonic force along the z-direction. The measurements of force and displacement of individual trajectories were saved every 10 fs. From these recorded trajectories, we derived the potential of mean force profiles using weighted histogram analysis method (WHAM) [64,65], which was used for calculation of ΔG_d.

2.7. Surface hydrophobicity and electrostatic potential analysis

The surface hydrophobicity of albumin and Dex-K/E4-OVA323 was represented by coloring the amino acids according to the Eisenberg scale using a modified color_h python script (green-white scale). Dexamethasone was colored in green to account for its high hydrophobicity. The surface electrostatic potential of albumin and Dex-K/E4-OVA323 were calculated using the APBS (Adaptive Poisson–Boltzmann Solver) software [66]. In brief, the PDB files of albumin and Dex-K/E4-OVA323 were converted to PQR files using PDB2PQR [67]. Subsequently, the PQR files were analyzed by APBS with default charges and atomic radii to generate the surface potential map. Structural representations were

prepared with either Pymol or Visual molecular dynamics (VMD, version 1.9.3, 68].

2.8. Native PAGE analysis

In vitro supramolecular complexation was performed by incubating 5 μM Dex-K/E4-OVA323 with 40% mouse plasma (abcam, Lot#GR3315537–2) in 1 × PBS at 37 °C for one hour. Subsequently, the mixtures were analyzed using NativePAGE™ 4–16% Bis-Tris gel (Thermo Fisher) running with 1× Tris-acetate-EDTA buffer. Dex-K/E4-OVA323 were Cy5-labeled via the addition of Fmoc-Lys(sulfo-Cy5)-OH (AAT Bioquest) to the N-terminal of the OVA323 sequence during the solid phase synthesis (i.e., Dex-K/E4-$K_{(Cy5)}$OVA323, Note S4–5). To minimize the effect of dye addition on the peptide chemical properties, instead of labeling one of the peptide residues, we labeled the additional lysine next to charged residues [69]. 1mg/mL of Rhodamine Green™-X NHS ester labeled (ThermoFisher, 1:1 ratio) mouse serum albumin (abcam, Lot#GR3387618–1) was added to the mixtures (10% of the total volume). Thereby, the distribution of Dex-K/E4-OVA323 and albumin in the 40% mouse plasma can be identified by fluorescence signal (Alexa488 filter for albumin, Cy5 filter for Dex-K/E4-OVA323) detected by ChemiDoc Imaging System (Bio-Rad Laboratories).

2.9. Mice

C57/BL6J wild-type female mice were purchased from InVivos (Singapore). Female C57BL/6-Ly5.1 and C57BL/6-Tg(TcraTcrb) 425Cbn/Crl (OTII) mice (8 weeks) were purchased from Charles River and kept under standard conditions at the animal facility. All studies were approved by the National University of Singapore Institutional Animal Care and Use Committee (IACUC) or the Animal Experiment Committee of Utrecht University under acquired license (CCD number: AVD108002016467; work protocol number: 467–3-05). The practice was conformed to the guidelines on the care and use of animals for scientific purposes (NACLAR, Singapore, 2004) and the Guide for the Care and Use of Laboratory Animals published by the US National Institutes of Health (NIH Publication, 8th Edition, 2011).

2.10. *Ex vivo fluorescence imaging*

The C57BL/6 J mice were s.c. injected with 200 μg Dex-K/E4-OVA323-Cy5, 140 μg OVA323-Cy5 or 1 × PBS via the two flanks (100 μL in 1 × PBS, 50 μL each side). The draining inguinal LNs, livers, and spleens were harvested 4 h after administration and imaged using the IVIS Spectrum In Vivo Imaging System as previously described [70] (PerkinElmer). Images were processed and quantified using the IVIS software.

2.11. Flow cytometry

As described before, single-cell suspension preparation, cell staining, and flow cytometry analysis were performed [71,72]. Briefly, lymph nodes were minced with a sharp blade, left lobe of the liver was minced with sharp scissors in 1 mL of digestion buffer RPMI supplemented with a cocktail of 1 mg/mL type II collagenase (Worthington Biochemical Corporation, Lakewood, NJ, USA) and 100 U/mL DNase I (Sigma-Aldrich), and digested for 45 min at 37 °C. Digested tissue samples were passed through a 19G syringe 5–10 times to complete digestion and filtered through a 100 μM cell strainer (BD Falcon, USA). Cells were dispersed by adding staining buffer (2% FBS in PBS) and spun down at 450 *g* for 5 min (4 °C). The cell pellet was resuspended in 10 mL of staining buffer, 1 mL of liver cells was stained for FACS analysis. For draining inguinal LNs, all cells were stained for FACS analysis (Table S1).

To block nonspecific antibody binding, cells were incubated with FC-block (Supernatant of 2.4G2 cells) for 5 min at 4 °C. Afterward, cells were incubated with an antibody cocktail for 30 min on ice in the dark. The list of antibodies is provided in Supplementary Table 1. Data was acquired using a Fortessa flow cytometer (Beckman Coulter) and analyzed with FlowJo (version 10.7.1). Macrophages were defined as $CD45^+Ly6G^-F4/80^+$, dendritic cells were defined as $CD45^+Ly6G^-CD3^-F480^-CD11C^+$, and Fluorescence minus one (FMO) was used as background control.

2.12. OTII adoptive transfer model for tolerogenic assay

On day −1, OTII mice were sacrificed. $CD4^+$ T cells were isolated from the spleen of OTII mice using a $CD4^+$ T-cell magnetic bead isolation kit (Miltenyi Biotec). A total of 5.5×10^5 $CD45.2^+CD4^+$ OT-II T cells were adoptively transferred into each $CD45.1^+$ Ly5.1 mouse via tail-vein injection. On day 0, samples (200 μg) were s.c. injected to both right and left flank of the Ly5.1 mouse (50 μL each in 1× PBS). The administered dose of Dex-K/E4-OVA323 was equivalent to an effective dose of 28 μg dexamethasone per mouse. Mice were sacrificed on day 7. The spleens of the different mice were isolated, and the splenocytes were analyzed by flow cytometry (Fig. S9, Table S1).

2.13. *Statistical analysis*

Statistical analysis was performed in GraphPad Prism v.9.1.1 using one-way ANOVA with Turkey's multiple comparison test. Data were presented as average ± standard deviations unless otherwise indicated. Significant statistical difference was annotated as * $p < 0.05$, ** $p < 0.01$, *** $p < 0.001$.

3. Results and discussion

3.1. Molecular design and synthesis

Dexamethasone was conjugated to the N-terminus of the K4-OVA323 and E4-OVA323 sequence via a carboxylesterase-sensitive succinyl-linker, which is a commonly utilized linker in peptide-drug conjugates [48–50]. To emulate vaccine epitopes flanked with cationic [45–47] or anionic [43,44] residues, four residues repeat of K or E were extended from the N-terminus of the OVA323 epitope (Fig. 1b, S1). Amino acids K and E were chosen as the cationic and anionic counterparts, respectively, as they have comparable molecular weights (K:146.2 Da, E:147.1 Da) and are commonly employed as charge counterparts in peptide material design [73,74]. Since albumin possesses a net negative charge under physiological conditions [20], the charge variation can cover the range of electrostatic interactions from attractive to repulsive. Besides, as the nonspecific albumin association possesses high heterogeneity [75], we limited the number of study candidates to two cognate candidates with opposing charges in order to navigate the charge effect towards albumin association dexamethasone-antigen conjugates and, at the same time, stayed focused on our study objective by not generating an overwhelming amount of data. Furthermore, conjugation of dexamethasone to peptide sequence can significantly increase its hydrophobicity, thereby heightening the propensity for the peptide to form β-sheet aggregates [76] and potentially altering the biodistribution and immunological profile [77]. To eliminate this variable in this study, the charged residues glutamate and lysine were added next to dexamethasone to prevent the formation of β-sheet aggregates [78]. The circular dichroism measurement confirmed that Dex-K/E4-OVA323 adopted an α-helical, rather than β-sheet, secondary structure (Fig. S8).

3.2. *De novo structure of mouse serum albumin and Dex-K/E4-OVA323*

To afford a better correlation between the computation and experimental work, we opted to maintain species consistency (mouse) throughout this study. However, there is currently no experimentally resolved structure of mouse serum albumin available in the protein data

bank. Deep-learning artificial intelligence methods offer a new possibility to bridge this knowledge gap, by which highly accurate atomic structures can be derived via de novo prediction (e.g., RoseTTAFold [52]). The generated RoseTTAfold model of albumin has a predicted local distance difference test (lDDT) of 0.9 at a scale of 0.0 (bad prediction) to 1.0 (good prediction), which underscores the high model confidence of the predicted structure [53]. The albumin structure consisted of three homologous domains (I:1–230, II: 231–422, III:423–608), which can be further divided into subdomain A and B according to their structural motifs (Fig. 2a, S2a). Furthermore, the mouse serum albumin is structurally arranged as a heart-shaped molecule with a dimension of ~8 × 8 × 3 nm. Interestingly, all these structural properties are similar to that of the human serum albumin [79] (Fig. S3), which is likely attributed to their high degree of sequence homology [80].

To study the structural properties of the dexamethasone-antigen conjugates, we used a de novo structure prediction software program, PEP-FOLD3 [54,55], to derive the most probable molecular conformations of the short peptide sequences (5 to 50 amino acids). Since small-molecule N-terminal modifications generally have limited influence over the final secondary structure of a short peptide sequence [81], the K/E4-OVA323 sequences were used for the de novo prediction. The best model of K4-OVA323 and E4-OVA323 showed that they adopt α-helical structure throughout the sequence (Fig. 2b, S2c-d). Next, the LigParGen [51] parameterized dexamethasone succinate was added to the N-terminus of the K/E4-OVA323 atomic model as an artificial amino acid (Fig. 2b). The dexamethasone-antigen conjugates have a dimension of ~1.5 × 1.5 × 3.5 nm. The small molecular size [11–13] of Dex-K/E4-OVA323 showed that a physiological transport mechanism is required to facilitate their distribution to the biologically active sites (i.e., lymph nodes [15–17], liver [18,19]).

3.3. The charged residue repeats in Dex-K/E4-OVA323 mediate albumin surface association

CG-MD simulations were performed to study the molecular parameters governing the association between albumin and Dex-K/E4-OVA323 at an affordable computation cost. The recently re-parameterized Martin 3.0 force field [58] was used for the CG-MD simulations, as it can accurately sample protein-small molecule drug interactions without a priori knowledge [57]. Furthermore, CG-MD simulations were chosen against the molecular docking-based methods to account for the conformational flexibility of the Dex-K/*E*-OVA323 in an aqueous environment [82], the internal motion of albumin due to its tertiary structures [83], and its better suitability to sample configurations for the nonspecific associations between Dex-K/E4-OVA323 and albumin [23,40,75,79]. Two independent trajectories were performed per sample. The final trajectories showed that Dex-K/E4-OVA323 were appended to the subdomain IIB and IIIA of albumin (Fig. 3), and the association sites are different between the two trajectories. The lack of convergence between the sampled configurations illustrates their good representation of the nonspecific association between Dex-K/E4-OVA323 and albumin [23,39,40,79] and is potentially related to the changes in albumin structural flexibility due to the association of Dex-K/E4-OVA323 [84]. Furthermore, in all four sampled configurations, we did not observe the insertion of Dex-K/E4-OVA323 into the hydrophobic binding pockets of albumin, as with some small-molecule drugs [15,23,79] (Fig. 3). The hydrophobic binding pocket is situated towards the core of the albumin subdomains [79]. Insertion of the dexamethasone moiety into the hydrophobic binding pockets is seemingly hindered by the hydrophilicity of the adjacent K/E4-OVA323 sequences, which are shown to be interacting with the surface residues in albumin (Figs. 3 and 4a). These results illustrate that albumin surfaces are the prime association sites between albumin and Dex-K/E4-OVA323, with lower specificity but higher capacity than hydrophobic pocket binding [75].

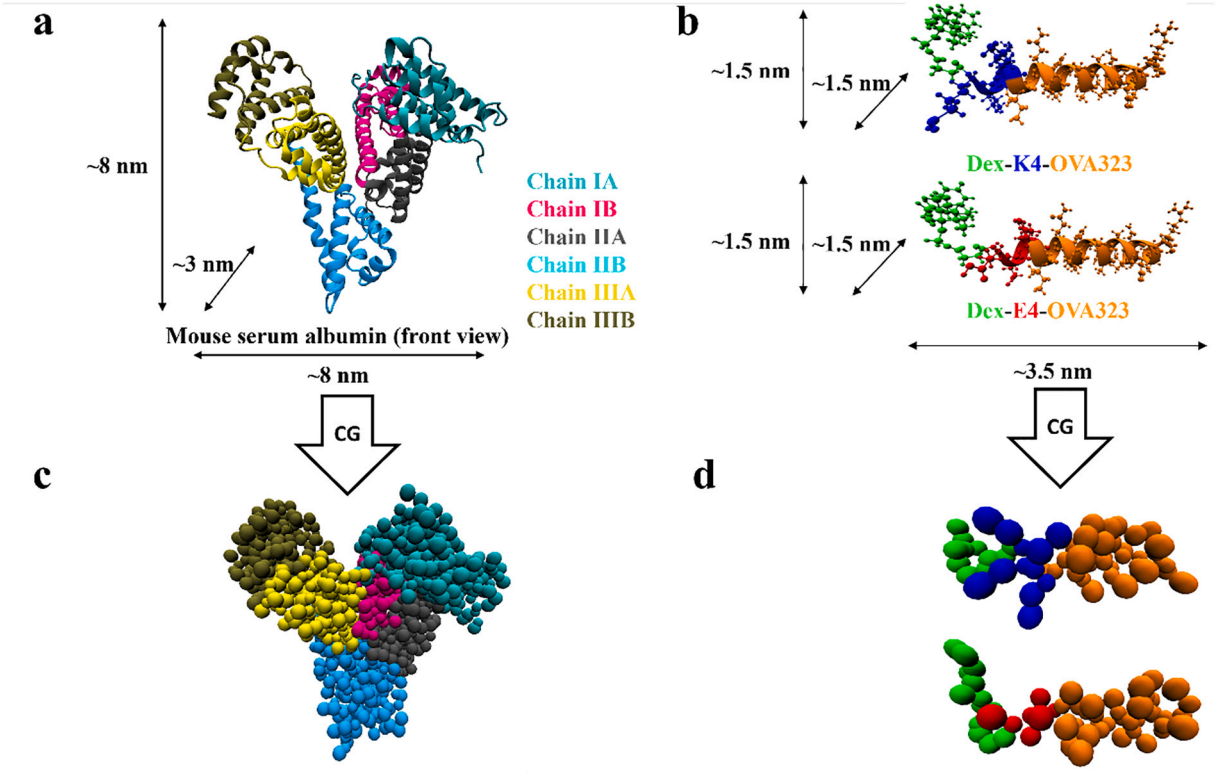

Fig. 2. De novo structures of mouse serum albumin and Dex-K/E4-OVA 323. (a) Dimensions and structural properties of the RoseTTAFold [52] model of mouse serum albumin. (b) Dimensions of PEP-FOLD3 [54] model of Dex-K/E4-OVA323. (c-d) The martini 3.0 [58] coarse-grained (CG) model of the albumin and Dex-K/E4-OVA323 derived from their respective atomistic models.

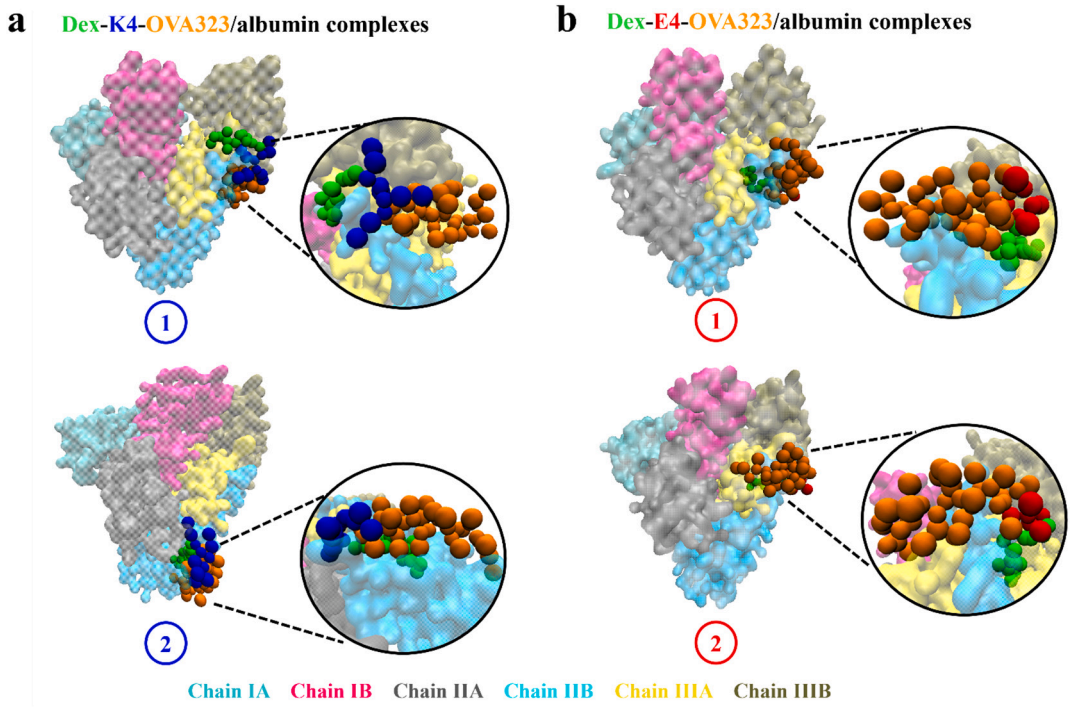

Fig. 3. CG-MD sampled configurations of Dex-K/E4-OVA-323 and albumin complexes. The configurations of the Dex-K/E4-OVA323 and albumin complexes were sampled upon 2 μs CG-MD simulations between one Dex-K/E4-OVA323 and one albumin. Two configurations are sampled per conjugate: (a) the complexes between Dex-K4-OVA323 and albumin; (b) the complexes between Dex-E4-OVA323 and albumin. The complexes' configuration showed that the dexamethasone moiety of Dex-K/E4-OVA323 does not insert deeply into the hydrophobic pockets of albumin but instead associates to surface hydrophobic patches of albumin.

Therefore, the albumin transport of Dex-K/E4-OVA323 is governed by their nonspecific association, which importance has gained increasing clinical awareness [25–27].

3.4. Generic dissociation pattern of complexes between Dex-K/E4-OVA323 and albumin

Next, the molecular properties of the complexes between Dex-K/E4-OVA323 and albumin were investigated using SMD simulations (Fig. 4a, S4). All Dex-K/E4-OVA323-albumin complexes followed a generic pattern of dissociation —1) the OVA323 sequences detached from the albumin surface (orange arrow in Fig. 4a); 2) the four repeats of charged residues (K4 or E4) detached from their oppositely charged residues in albumin (blue or red arrow in Fig. 4a); 3) the dexamethasone moiety detached from the residues to liberate the Dex-K/E4-OVA323 conjugates (green arrow in Fig. 4a). This generic dissociation pattern can also be discerned in the force-time plots of the SMD trajectories (Fig. 4b), which records the build-up and rupture of pulling forces in the virtual harmonic spring of Dex-K/*E*-OVA323. In all these four force-time plots, the primary force rupture took place when the accumulated pulling forces were sufficient to overcome the OVA323-albumin interactions (orange line in Fig. 4b); a subsequent secondary force rupture took place when the K4- or E4-albumin interactions were overcome by the accumulated pulling forces (blue or red line in Fig. 4b); finally, a tertiary force rupture took place when the accumulated pulling forces overcame the dexamethasone-albumin interactions (green line in Fig. 4b). The triphasic dissociation profile shows that the dexamethasone moiety is the primary driver for the Dex-K/E4-OVA323 and albumin association. This indicates there is high plausibility for Dex-K/E4-OVA323 and dexamethasone sharing the same mode of physiological transport (i.e., albumin as carrier protein) [38,39]. Furthermore, the rupture of K4- and E4-albumin interactions has the highest variability in magnitude among these three phases of force rupture (e.g., ~600 kJ mol^{-1} nm^{-1} for K4-albumin in configuration ①; ~300 kJ mol^{-1} nm^{-1} for E4-albumin in configuration ②). This magnitude variation in interaction forces, in turn, dictates the resultant dissociation energy (ΔG_d, Fig. 4a, S5), which further substantiates the critical role of charged residues adjacent to the drug conjugation site in the association process. Finally, the magnitude of ΔG_d is comparable between Dex-K4-OVA323 and Dex-E4-OVA323 (Fig. 4a). This shows that Dex-K4-OVA323 and Dex-E4-OVA323 display similar albumin association properties in an isolated one-to-one context.

3.5. Evaluation of albumin surface properties governing the association capacity for Dex-K/E4-OVA323

Despite having lower affinity than typical ligand-receptor interactions, the prevalence of nonspecific albumin association in the physiological environment is originated from their essentially higher interaction capacity [25–27,75]. Therefore, a more comprehensive approach should be utilized to study the nonspecific albumin association with Dex-K/E4-OVA323. The CG-MD studies above show that surface-exposed hydrophobic and charged patches are essential for the nonspecific association of Dex-K/E4-OVA323 to albumin. Consequently, a survey over the surface hydrophobicity and electrostatic potential of albumin can effectively characterize the albumin association capacity of these dexamethasone-antigen conjugates (Fig. 5). According to the Eisenberg scales, the surface amino acids of albumin were colored by their hydrophobicity [85]. The colorimetric representation showed that hydrophobic patches are present across the albumin surface (Fig. 5a), which shared a high level of similarity with the human serum albumin (Fig. S3a). Surface hydrophobic patches are essential for albumin to execute its biological duties [86], e.g., scavenging hydrophobic toxins and fatty acids [36], ensuring albumin has ample reception sites for the hydrophobic association of Dex-K/E4-OVA323. Furthermore, surface hydrophobicity evaluation of Dex-K/E4-OVA323 showed that the OVA323 sequence possesses a moderate hydrophobicity, and the hydrophobic residues are much less exposed than the dexamethasone

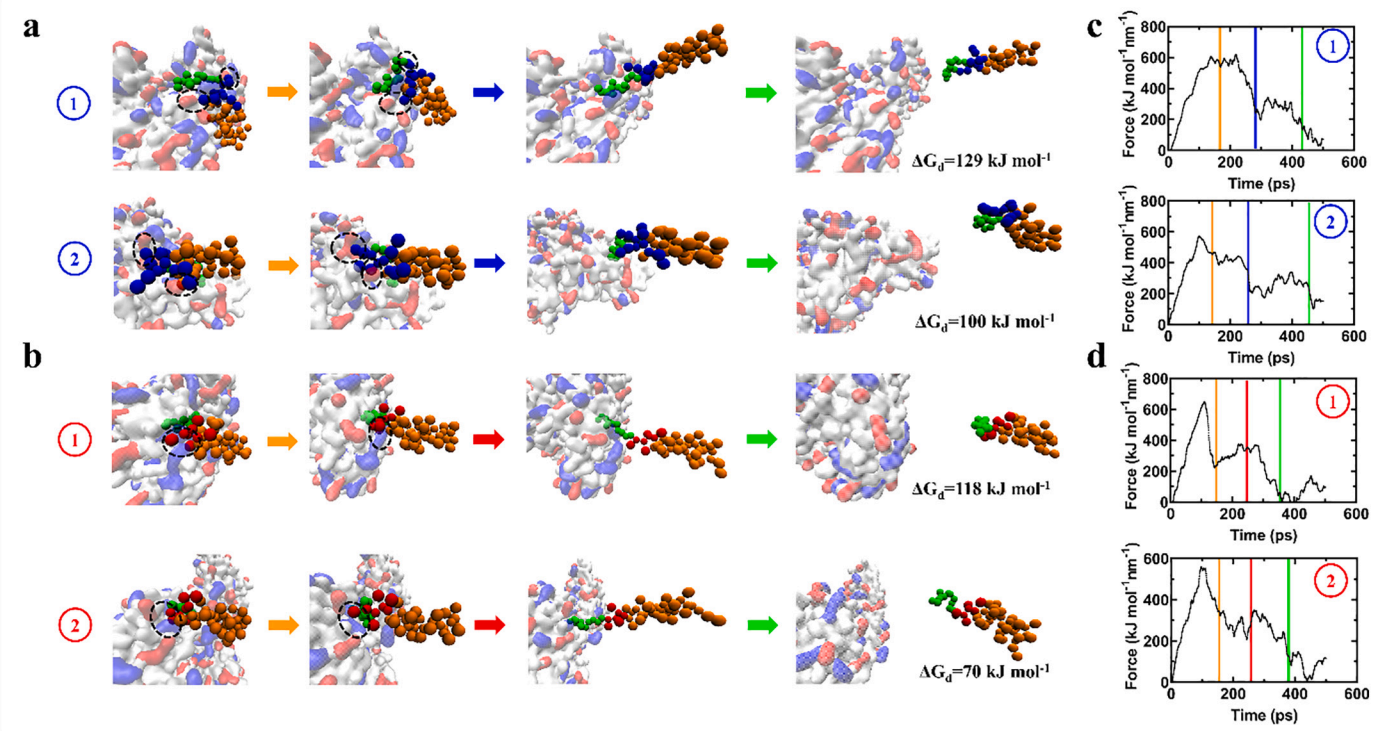

Fig. 4. Generic dissociation pattern of complexes between Dex-K/E4-OVA-323 and albumin. Trajectories of the SMD simulations highlighting the triphasic dissociation pattern of complexes between (a) Dex-K4-OVA323 and albumin and (b) Dex-E4-OVA323 and albumin: 1) dissociation of OVA323 sequence (orange arrow); 2) dissociation of the four charged residues repeat (red or blue arrow); and dissociation of the dexamethasone moiety (green arrow). Each configuration's dissociation energy (ΔG_d) was calculated from the PMF profiles derived using WHAM [64,65]. The magnitude of the ΔG_d correlates to the number of complementary electrostatic sites on the albumin surface (circled in dotted line). The force-time plots of the SMD trajectories between (c) Dex-K4-OVA323 and albumin and (d) Dex-E4-OVA323 and albumin also captured the triphasic dissociation pattern. Each force rupture event corresponds well to the moieties dissociating from the albumin (orange line: OVA323, blue or red line: K/E4, green: dexamethasone). (For interpretation of the references to colour in this figure legend, the reader is referred to the web version of this article.)

moiety (Fig. 5a). Therefore, it further endorses the leading role of dexamethasone in driving the hydrophobic association of Dex-K/E4-OVA323 to albumin.

Next, the electrostatic surface potential map of the albumin and Dex-K/E4-OVA323 were calculated using the Adaptive Poisson-Boltzmann Solver (APBS) program [66] to assess the reception sites for complementary electrostatic interactions. In agreement with the literature [20], albumin displays a dominant anionic surface charge with a blend of several scattered cationic regions (Fig. 5b), which resemble the features of human serum albumin (Fig. S3c). This shows that the complementary electrostatic sites on albumin surfaces are more abundant for Dex-K4-OVA323 than Dex-E4-OVA323. Conversely, the electrostatic repulsion sites on the albumin surface are more abundant for Dex-E4-OVA323 than Dex-K4-OVA323, in which the repulsive force can serve as a thrust to reverse the hydrophobic association of the dexamethasone-antigen conjugates.

3.6. *In vitro validation of albumin association capacity of Dex-K/E4-OVA323*

Next, native PAGE analysis was performed to validate the effect of surface properties of the Dex-K/E4-OVA323 on the albumin association capacity. Since s.c. injection is the chosen route of administration in the animal studies (discussed below), 40% murine plasma in 1 × phosphate-buffered saline (1 × PBS) was used to simulate the biofluid of the s.c. tissue in the native PAGE studies [87]. Dex-K/E4-OVA323-Cy5 (5 μM) and albumin-RhoG (100 μg/mL) were incubated in the simulated s.c. fluid at 37 °C for 1 h before the native PAGE analysis. Due to the cationic charges of Dex-K4-OVA323, the Dex-K4-OVA323-Cy5 in PBS did not migrate into the gel (sample 1, Fig. 5c) but did so when Dex-K4-OVA323 was incubated with 40% plasma, presumably due to complexation with plasma proteins that will also be present in the s.c. fluid (sample 4, Fig. 5c). Furthermore, Dex-K4-OVA323-Cy5 colocalized with the albumin-RhoG band (sample 4, Fig. 5c), while the Dex-E4-OVA323-Cy5 band migrated quicker than the albumin-RhoG band (sample 5, Fig. 5c). This validates that Dex-K4-OVA323 possesses a higher albumin association capacity than Dex-E4-OVA323. Besides, it shows that the E4-albumin electrostatic repulsion forces are likely triggering the unbinding events. Furthermore, the Dex-E4-OVA323-Cy5 in the PBS band (sample 2, Fig. 5c) migrated slower than the Dex-E4-OVA323-Cy5 band in 40% murine plasma (sample 5, Fig. 5c). The large apparent molecular weight (~21–63 kDa) of the Dex-E4-OVA323-Cy5 in PBS is likely caused by the formation of oligomeric assemblies [88]. The difference in the band migration between these two samples illustrates that, despite not forming detectable complexes with Dex-E4-OVA323, the plasma proteins act as a physiological solubilizer [89] to lower the size of oligomeric assemblies of Dex-E4-OVA323 (<21 kDa, Fig. 5c). Interestingly, our results deviate from previous findings with lipid-modified peptide conjugates, in which anionic residues adjacent to the conjugation sites enhance the albumin association of these peptide conjugates [16,90]. This discrepancy can be explained by the ability of these extended moieties to insert into the albumin hydrophobic binding pocket [16,90], in which the mode of albumin association is different from dexamethasone-antigen conjugates (i.e., association to albumin surface). Hence, it illustrates that the molecular extensiveness (i.e., chain vs. ring) of the albumin interaction moiety plays an important role in governing the albumin association properties of the peptide conjugates [16,90]. Finally, to demonstrate the translatability of our current findings to later clinical development, we performed native PAGE analysis with human serum albumin, which showed comparable results with

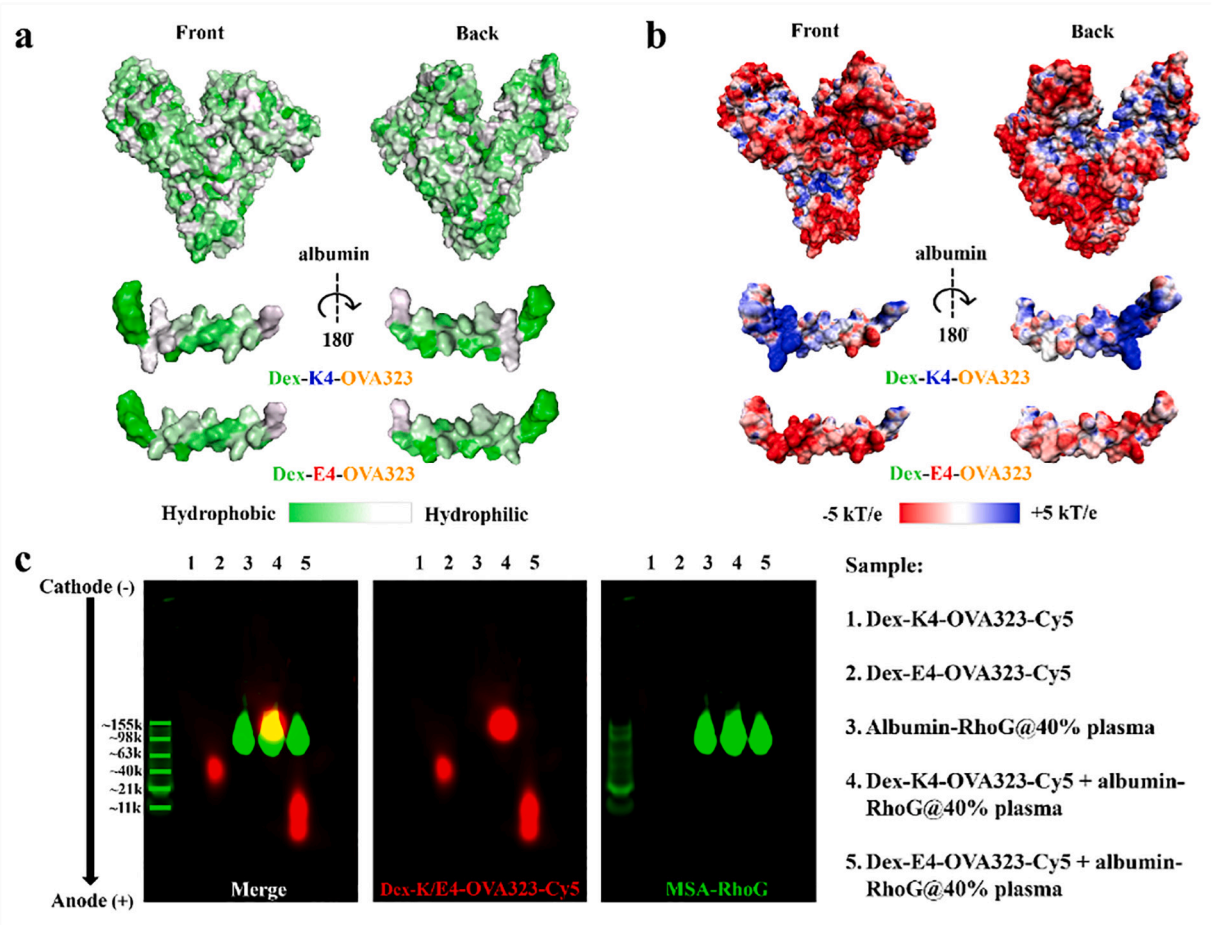

Fig. 5. In silico evaluation and in-situ validation of the albumin association capacity of Dex-K/E4-OVA-323. (a) Surface hydrophobicity (according to Eisenberg scale in green-white scale); and (b) surface electrostatic potential (calculated with APBS [66], visualized as isocontours at −5 kT/e, red and + 5 kT/e, blue) representation of albumin and Dex-K/E4-OVA323. (c) In-situ validation of the albumin association capacity of Dex-K/E4-OVA-323 using native PAGE analysis. Structural representations were prepared with pymol or VMD software [68]. (For interpretation of the references to colour in this figure legend, the reader is referred to the web version of this article.)

mouse serum albumin (Fig. S9).

3.7. Enhanced retention and uptake by antigen-presenting cells of s.c. administered Dex-K4-OVA323

To determine how the difference in albumin association capacity of dexamethasone antigen conjugates can influence the antigen-specific tolerogenic response, we investigated the in vivo trafficking of Dex-K/E4-OVA323 conjugates to the biologically active sites, lymph nodes [15–17], and liver [18,19]. Dex-K/E4-OVA323 conjugates were administered via s.c. injection in this study, in which the absence of carboxylesterases in the subcutaneous tissue can offer an inert environment to preserve the molecular integrity of Dex-K/E4-OVA323 before association with albumin [91,92]. Four hours post-administration of Cy5-labeled Dex-K/E4-OVA323 or OVA323 to C57BL/6 J mice, the three major induction sites of antigen-specific Treg [10,19], the draining inguinal lymph node (LN), liver, and spleen, were collected for imaging analysis with an IVIS Spectrum optical imager.

As shown in Fig. 6a, the fluorescence intensity of Dex-E4-OVA323 and OVA323 in the inguinal LN, liver, and spleen was negligible. In contrast, the fluorescence intensity of Dex-K4-OVA323 in the three organs was markedly higher, indicating Dex-K4-OVA323 has better retention to the biologically active sites upon s.c. administration. These results illustrate that the higher albumin association capacity of the dexamethasone-antigen conjugates can lead to enhanced accumulation in their biologically active sites. These results stand in good agreement with the literature that conjugation of albumin-binding molecules to peptides can enhance their lymphatic and hepatic retention in vivo [15–17,35].

Given that APC (macrophages and dendritic cells) processing of the dexamethasone-antigen conjugates is crucial for the induction of antigen-specific Treg, the uptake of Dex-K/E4-OVA323 conjugates by macrophages and dendritic cells in the inguinal LN, liver, and spleen was analyzed at the single-cell level using flow cytometry. In the inguinal LNs, macrophages showed significantly higher uptake of Dex-K4-OVA323 compared to Dex-E4-OVA323, whereas dendritic cells exhibited similar uptake of Dex-K4-OVA323 and Dex-E4-OVA323 (Fig. 6b). However, uptake by macrophages and dendritic cells in the liver was higher for Dex-K4-OVA323 than Dex-E4-OVA323 (Fig. 6c). Besides, there is no significant difference in APC uptake in the spleen between all injected samples (Fig. 6d). Taken together, the overall APC uptake of Dex-K4-OVA323 was significantly higher in the liver (~18–38% $Cy5^+$ APCs) than that in the inguinal LNs (~0.4–1.2% $Cy5^+$ APCs) and spleen (~0.25–2.65% $Cy5^+$ APCs), which the level of lymphatic and splenic APC uptake is considerably low compared to other lymphatic and splenic targeting peptide materials [73]. This shows that the liver, rather than inguinal LNs and spleen, is the primary site for APC processing of the dexamethasone-antigen conjugates. Taking reference to the trajectory of metabolite transport by albumin, after sequestering drugs or toxins from around the body (e.g., subcutaneous tissue), the albumin is transported to the liver (e.g., via lymphatic system) for processing before being recycled into the blood circulation [93]. These results suggest that

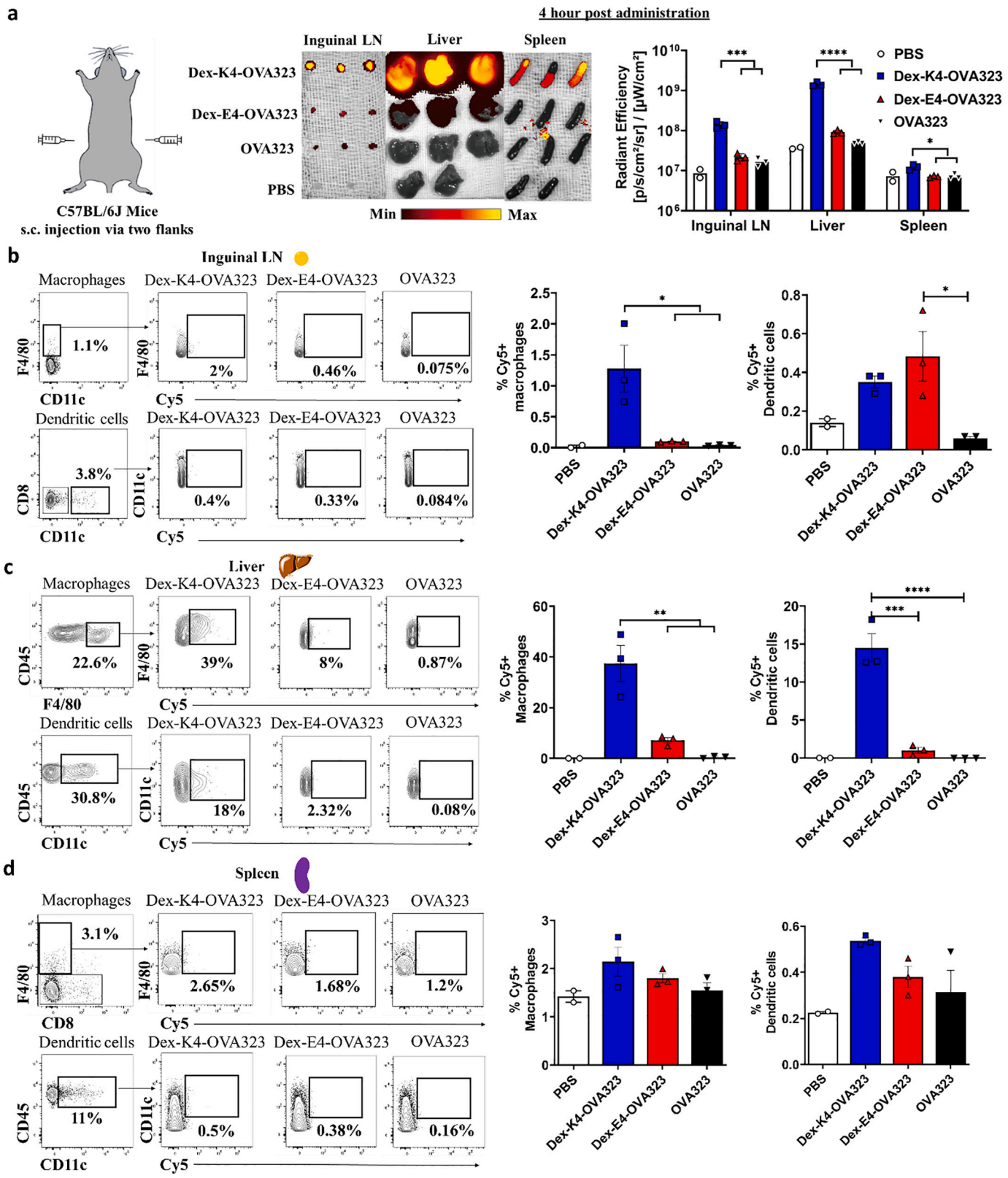

Fig. 6. Biodistribution and cell uptake of Dex-K/E4-OVA-323 upon s.c. injection. (a) Mice were s.c. injected with 200 μg Dex-K/E4-OVA323-Cy5, 140 μg OVA323-Cy5 or PBS (100 Ll in total, 50 Ll per flank). The draining inguinal lymph node (LN), liver, and spleen were collected 4 h post-administration. Subsequently, the fluorescent signal in the organs was imaged and quantified by an IVIS imaging system and software (b-d). Flow cytometry analysis of fluorescent peptide uptake by macrophages and dendritic cells in the (b) inguinal LN, (c) liver, and (d) spleen. Data were analyzed by one-way ANOVA with Turkey's test and expressed as the mean ± standard deviations ($n = 3$; $n = 2$ for PBS); * $p < 0.05$, *** $p < 0.001$, ****$p < 0.0001$.

Dex-K4-OVA323 follows this albumin transport trajectory, in which the lymphatic system serves a transition role for the hepatic transport of albumin/Dex-K4-OVA323 complexes.

3.8. Dex-K4-OVA323 specifically expands the OVA323-specific Treg population

To assess the correlation between the albumin association capacity and the OVA323-specific tolerogenic response of Dex-K/E4-OVA323, an OVA323 specific adoptive transfer model (OTII) was employed [94] (Fig. 7a). Each host C57BL/6-Ly5.1 mouse (CD45.1$^+$ phenotype, non-OVA323 specific) received an injection of OTII CD4$^+$ T cells (CD45.2$^+$ phenotype, OVA323 specific) one day before administering the samples (day −1). On day 0, mice received s.c. injection of Dex-K/E4-OVA323 or OVA323 epitope for vaccination, or 1 × PBS as blank control. Since the spleen, the largest secondary lymphoid organ, is essential for maintaining hepatic immunotolerance [19] and is often employed to assess the systemic antigen-specific immunotolerance [3,95], we analyzed splenic CD4$^+$ T cells by flow cytometry on day 7 post-vaccination. As shown in Fig. 7b, neither Dex-K4-OVA323 nor Dex-E4-OVA323 exerted a pronounced effect on Treg population in Ly5.1 mice (host: CD45.2$^-$CD25$^+$Foxp3$^+$ and donor: CD45.2$^+$CD25$^+$Foxp3$^+$). Since free dexamethasone can directly expand the overall Treg population in a non-antigen-specific manner [96,97], this result suggests the amount of dexamethasone released from Dex-K/E4-OVA323 conjugates in the physiological environment was biologically negligible. However, further analysis of OVA323-specific T cells (donor: CD4$^+$CD45.2$^+$) revealed a remarkable expansion of Treg cells in the mice treated with Dex-K4-OVA323, but not Dex-E4-OVA323 or OVA323 epitope, compared to the mice receiving PBS (Fig. 7c). Despite Dex-K4-OVA323 exhibiting higher splenic accumulation than Dex-E4-OVA323 and OVA323 upon s.c. injection, there is no significant difference in their splenic APC uptake (Fig. 6d). Thus, this shows that the level of splenic OVA323-specific Treg is correlated to the hepatic, rather than splenic,

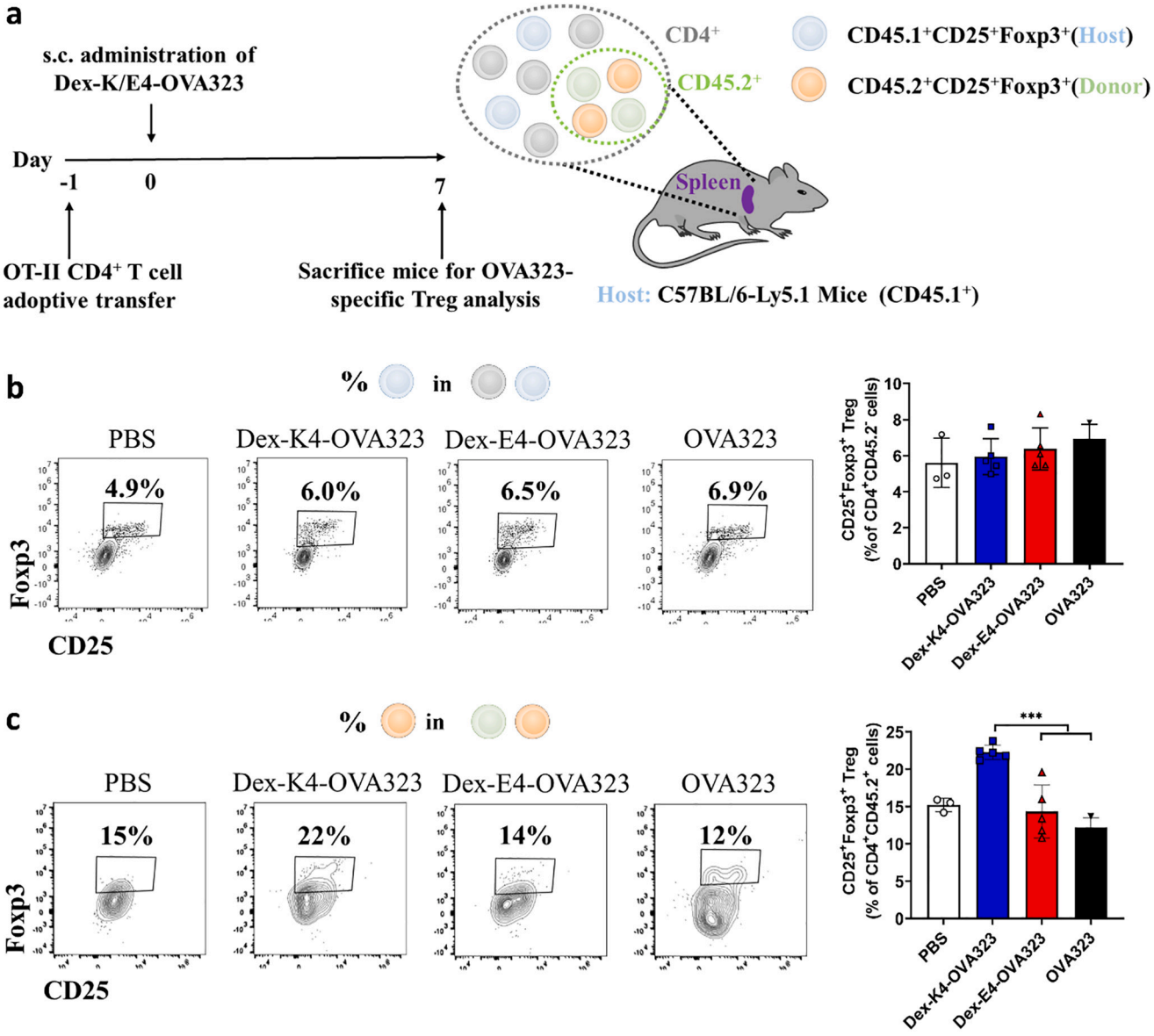

Fig. 7. Induction of OVA323-specific tolerance by Dex-K/E4-OVA-323. a) The CD45.1$^+$ C57BL/6-Ly5.1 mice received an adoptive transfer of OTII CD45.2$^+$CD4$^+$ T cells on day −1. The Ly5.1 mice were treated with phosphate-buffered saline (PBS, control), 200 μg of Dex-K/E4-OVA323, or OVA323 epitope via s.c. injection to both flanks (50 Ll each). The mice were sacrificed on day 7, and the spleen was harvested for flow cytometry analysis. b) Percentage of Treg (CD25$^+$Foxp3$^+$) in CD4$^+$CD45.2$^-$ T cells. c) Percentage of Treg in OTII CD45.2$^+$ T cells. Data were analyzed by one-way ANOVA with Turkey's test and expressed as the mean ± standard deviations ($n = 5$; $n = 3$ for PBS); *** $p < 0.001$.

accumulation of the dexamethasone-antigen conjugates [19]. Overall, these results indicate that OVA323-specific Treg induction is enhanced by higher albumin association capacity of the dexamethasone-antigen conjugate attributable to the cationic K4 rather than anionic E4 residues adjacent to the drug conjugation site.

Overall, our findings can serve as a guide to augmenting the induction of Treg amid replacing vaccine epitope sequences in dexamethasone-antigen conjugates, which is necessary for future development of autoimmune disease treatment, such as atherosclerosis [4,5], and Type I Diabetes [2,6]. In particular, for vaccine epitopes with anionic residues next to the dexamethasone conjugation sites, one should consider extending the sequence with cationic residues, as we demonstrated with Dex-K4-OVA323, or switching conjugation sites with flanking cationic residues [45–47]. In addition, the differential biodistribution profiles steered by charged residues adjacent to the drug conjugation sites present a potential design consideration for future development of peptide-drug conjugates, in which the flanking residues can be altered to enhance the albumin-assisted delivery for application such as targeted tumor delivery [24,98]. Besides, implications of our findings could be extended to protein-drug conjugates, e.g., antibody-drug conjugates [99], which have multiple drug conjugation sites. The generic properties of residues flanking the drug conjugation sites can potentially affect their interaction with physiological proteins, e.g., albumin, enzyme. Finally, having shown that dexamethasone-antigen conjugate with high albumin association capacity can selectively upregulate antigen-specific Treg in the spleen, autoimmune diseases with a direct link to splenic immunity should be chosen for preliminary investigations. For example, dexamethasone-antigen conjugates are a promising candidate for inducing antigen-specific Treg in the cardiosplenic axis for disease alleviation (e.g., myosin heavy chain $\alpha_{614–629}$-specific $CD4^+$ T cell activity after myocardial infarction) [100].

4. Conclusion

In summary, our findings showed that manipulating the charged residues (cationic or anionic) adjacent to the drug conjugation site in dexamethasone-antigen conjugates can markedly alter their albumin association capacity, thereby leading to a different biodistribution to the biologically active sites and induction of OVA323-specific Treg. We showed that cationic residues next to the drug conjugation sites in the dexamethasone-antigen conjugates could lead to a more robust tolerogenic response than the anionic residues counterparts. By that, our study can serve as a helpful guide for optimizing the tolerogenic response of dexamethasone-antigen conjugates amid a potential change of vaccine epitope sequences. Moreover, our findings demonstrated that altering the flanking residues next to the drug conjugation sites in peptide-drug conjugates can markedly modulate its biological outcome. Such a molecular engineering approach will benefit future peptide-drug conjugate development.

CRediT authorship contribution statement

Chun Yin Jerry Lau: Conceptualization, Data curation, Formal analysis, Investigation, Methodology, Project administration, Visualization, Writing – original draft, Writing – review & editing. **Naomi Benne:** Data curation, Formal analysis, Methodology, Resources. **Bo Lou:** Data curation, Formal analysis. **Olga Zharkova:** Data curation, Formal analysis, Methodology. **Hui Jun Ting:** Data curation, Formal analysis. **Daniëlle ter Braake:** Data curation, Formal analysis. **Nicky van Kronenburg:** Data curation, Formal analysis. **Marcel H. Fens:** Data curation, Formal analysis. **Femke Broere:** Data curation, Formal analysis, Methodology, Resources. **Wim E. Hennink:** Conceptualization, Funding acquisition, Methodology, Project administration, Resources, Supervision, Validation, Writing – review & editing. **Jiong-Wei Wang:** Conceptualization, Funding acquisition, Investigation, Methodology, Project administration, Resources, Supervision, Validation, Writing – review & editing. **Enrico Mastrobattista:** Conceptualization, Funding acquisition, Investigation, Methodology, Project administration, Resources, Supervision, Validation, Writing – original draft, Writing – review & editing.

Acknowledgment

We thank Alexandre M. J. J. Bonvin for critically reviewing the manuscript before submission; Danny Wilbie for his help with native PAGE analysis. The authors acknowledge financial support from the European Union Horizon 2020 NANOMED Grant 676137 to C.Y.J.L and E.M., and the National University of Singapore Nano NASH Program (NUHSRO/2020/002/NanoNash/LOA), the National University of Singapore Yong Loo Lin School of Medicine Nanomedicine Translational Research Program (NUHSRO/2021/034/TRP/09/Nanomedicine), and the MOE AcRF Tier 1 grant (NUHSRO/2021/113/T1/Seed-Sep/06) to J. W.W.

Appendix A. Supplementary data

Supplementary data to this article can be found online at https://doi.org/10.1016/j.jconrel.2022.06.025.

References

[1] S. Sakaguchi, M. Miyara, C.M. Costantino, D.A. Hafler, FOXP3+ regulatory T cells in the human immune system, Nat. Rev. Immunol. 10 (2010) 490–500.
[2] J.H. Esensten, Y.D. Muller, J.A. Bluestone, Q. Tang, Regulatory T-cell therapy for autoimmune and autoinflammatory diseases: the next frontier, J. Allergy Clin. Immunol. 142 (2018) 1710–1718.
[3] C. Krienke, L. Kolb, E. Diken, M. Streuber, S. Kirchhoff, T. Bukur, Ö. Akilli-Öztürk, L.M. Kranz, H. Berger, J. Petschenka, M. Diken, S. Kreiter, N. Yogev, A. Waisman, K. Karikó, Ö. Türeci, U. Sahin, A noninflammatory mRNA vaccine for treatment of experimental autoimmune encephalomyelitis, Science 371 (2021) 145.
[4] G.K. Hansson, J. Nilsson, Developing a vaccine against atherosclerosis, Nat. Rev. Cardiol. 17 (2020) 451–452.
[5] J. Nilsson, G.K. Hansson, Vaccination strategies and immune modulation of atherosclerosis, Circ. Res. 126 (2020) 1281–1296.
[6] A. Spence, W. Purtha, J. Tam, S. Dong, Y. Kim, C.-H. Ju, T. Sterling, M. Nakayama, W.H. Robinson, J.A. Bluestone, M.S. Anderson, Q. Tang, Revealing the specificity of regulatory T cells in murine autoimmune diabetes, Proc. Natl. Acad. Sci. 115 (2018) 5265.
[7] R.A. Maldonado, R.A. LaMothe, J.D. Ferrari, A.-H. Zhang, R.J. Rossi, P.N. Kolte, A.P. Griset, C. O'Neil, D.H. Altreuter, E. Browning, L. Johnston, O.C. Farokhzad, R. Langer, D.W. Scott, U.H. von Andrian, T.K. Kishimoto, Polymeric synthetic nanoparticles for the induction of antigen-specific immunological tolerance, Proc. Natl. Acad. Sci. 112 (2015) E156.
[8] R.W. Sands, I. Tabansky, C.S. Verbeke, D. Keskin, S. Michel, J. Stern, D. J. Mooney, Steroid–peptide immunoconjugates for attenuating T cell responses in an experimental autoimmune encephalomyelitis murine model of multiple sclerosis, Bioconjug. Chem. 31 (2020) 2779–2788.
[9] C.J. Pickens, M.A. Christopher, M.A. Leon, M.M. Pressnall, S.N. Johnson, S. Thati, B.P. Sullivan, C. Berkland, Antigen-drug conjugates as a novel therapeutic class for the treatment of antigen-specific autoimmune disorders, Mol. Pharm. 16 (2019) 2452–2461.
[10] A. Cifuentes-Rius, A. Desai, D. Yuen, A.P.R. Johnston, N.H. Voelcker, Inducing immune tolerance with dendritic cell-targeting nanomedicines, Nat. Nanotechnol. 16 (2021) 37–46.
[11] N.L. Trevaskis, L.M. Kaminskas, C.J.H. Porter, From sewer to saviour — targeting the lymphatic system to promote drug exposure and activity, Nat. Rev. Drug Discov. 14 (2015) 781–803.
[12] G.M. Ryan, L.M. Kaminskas, C.J.H. Porter, Nano-chemotherapeutics: maximising lymphatic drug exposure to improve the treatment of lymph-metastatic cancers, J. Control. Release 193 (2014) 241–256.
[13] M. Longmire, P.L. Choyke, H. Kobayashi, Clearance properties of nano-sized particles and molecules as imaging agents: considerations and caveats, Nanomedicine 3 (2008) 703–717.
[14] N. Bertrand, J.-C. Leroux, The journey of a drug-carrier in the body: an anatomo-physiological perspective, J. Control. Release 161 (2012) 152–163.
[15] M. Abdallah, O.O. Müllertz, I.K. Styles, A. Mörsdorf, J.F. Quinn, M.R. Whittaker, N.L. Trevaskis, Lymphatic targeting by albumin-hitchhiking: applications and optimisation, J. Control. Release 327 (2020) 117–128.
[16] H. Liu, K.D. Moynihan, Y. Zheng, G.L. Szeto, A.V. Li, B. Huang, D.S. Van Egeren, C. Park, D.J. Irvine, Structure-based programming of lymph-node targeting in molecular vaccines, Nature 507 (2014) 519–522.
[17] P. Yousefpour, A. Varanko, R. Subrahmanyan, A. Chilkoti, Recombinant fusion of glucagon-like Peptide-1 and an albumin binding domain provides Glycemic control for a week in diabetic mice, Adv. Therap. 3 (2020) 2000073.

[18] M. Raska, Z. Moldoveanu, J. Novak, Z. Hel, L. Novak, J. Bozja, R.W. Compans, C. Yang, J. Mestecky, Delivery of DNA HIV-1 vaccine to the liver induces high and long-lasting humoral immune responses, Vaccine 26 (2008) 1541–1551.

[19] A. Carambia, B. Freund, D. Schwinge, O.T. Bruns, S.C. Salmen, H. Ittrich, R. Reimer, M. Heine, S. Huber, C. Waurisch, A. Eychmüller, D.C. Wraith, T. Korn, P. Nielsen, H. Weller, C. Schramm, S. Lüth, A.W. Lohse, J. Heeren, J. Herkel, Nanoparticle-based autoantigen delivery to Treg-inducing liver sinusoidal endothelial cells enables control of autoimmunity in mice, J. Hepatol. 62 (2015) 1349–1356.

[20] G. Fanali, A. di Masi, V. Trezza, M. Marino, M. Fasano, P. Ascenzi, Human serum albumin: from bench to bedside, Mol. Asp. Med. 33 (2012) 209–290.

[21] M.P. Czub, B.S. Venkataramany, K.A. Majorek, K.B. Handing, P.J. Porebski, S. R. Beeram, K. Suh, A.G. Woolfork, D.S. Hage, I.G. Shabalin, W. Minor, Testosterone meets albumin – the molecular mechanism of sex hormone transport by serum albumins, Chem. Sci. 10 (2019) 1607–1618.

[22] M.P. Czub, K.B. Handing, B.S. Venkataramany, D.R. Cooper, I.G. Shabalin, W. Minor, Albumin-based transport of nonsteroidal anti-inflammatory drugs in mammalian blood plasma, J. Med. Chem. 63 (2020) 6847–6862.

[23] I.G. Shabalin, M.P. Czub, K.A. Majorek, D. Brzezinski, M. Grabowski, D.R. Cooper, M. Panasiuk, M. Chruszcz, W. Minor, Molecular determinants of vascular transport of dexamethasone in COVID-19 therapy, IUCrJ 7 (2020) 1048–1058.

[24] E.N. Hoogenboezem, C.L. Duvall, Harnessing albumin as a carrier for cancer therapies, Adv. Drug Deliv. Rev. 130 (2018) 73–89.

[25] T.S. Maurer, Nonspecific binding considerations in the rational design and development of small molecule COVID-19 therapeutics, Clin. Pharmacol. Therap. 110 (2021) 294–296.

[26] M. Boffito, D.J. Back, C. Flexner, P. Sjö, T.F. Blaschke, P.W. Horby, D. Cattaneo, E. P. Acosta, P. Anderson, A. Owen, Toward consensus on correct interpretation of protein binding in plasma and other biological matrices for COVID-19 therapeutic development, Clin. Pharmacol. Therap. 110 (2021) 64–68.

[27] F. Stanke-Labesque, D. Concordet, Z. Djerada, S. Bouchet, C. Solas, E. Mériglier, F. Bonnet, B. Mourvillier, S. Ruiz, G. Martin-Blondel, O. Epaulard, C. Schwebel, E. Gautier-Veyret, P. Gandia, Neglecting plasma protein binding in COVID-19 patients leads to a wrong interpretation of Lopinavir overexposure, Clin. Pharmacol. Therap. 109 (2021) 1030–1033.

[28] M. Ellmerer, L. Schaupp, G.A. Brunner, G. Sendlhofer, A. Wutte, P. Wach, T. R. Pieber, Measurement of interstitial albumin in human skeletal muscle and adipose tissue by open-flow microperfusion, Am. J. Physiol. Endocrinol. Metabol. 278 (2000) E352–E356.

[29] S. Miyauchi, M. Masuda, S.-J. Kim, Y. Tanaka, K.-R. Lee, S. Iwakado, M. Nemoto, S. Sasaki, K. Shimono, Y. Tanaka, Y. Sugiyama, The phenomenon of albumin-mediated hepatic uptake of organic anion transport polypeptide substrates: prediction of the in vivo uptake clearance from the in vitro uptake by isolated hepatocytes using a facilitated-dissociation model, Drug Metab. Dispos. 46 (2018) 259.

[30] J.H. Chang, Y.-C. Chen, J. Cheong, R.S. Jones, J. Pang, Investigating the impact of albumin on the liver uptake of Pitavastatin and warfarin in Nagase Analbuminemic rats, Drug Metab. Dispos. 47 (2019) 1307.

[31] S. Miyauchi, S.-J. Kim, W. Lee, Y. Sugiyama, Consideration of albumin-mediated hepatic uptake for highly protein-bound anionic drugs: bridging the gap of hepatic uptake clearance between in vitro and in vivo, Pharmacol. Ther. 107938 (2021).

[32] C. Ruan, L. Liu, Y. Lu, Y. Zhang, X. He, X. Chen, Y. Zhang, Q. Chen, Q. Guo, T. Sun, C. Jiang, Substance P-modified human serum albumin nanoparticles loaded with paclitaxel for targeted therapy of glioma, Acta Pharm. Sin. B 8 (2018) 85–96.

[33] Q. Wang, X. Guo, Y. Chen, Z. Wu, Y. Zhou, S. Sadaf, L. Han, X. Ding, T. Sun, Theranostics system caged in human serum albumin as a therapy for breast tumors, J. Mater. Chem. B 8 (2020) 6877–6885.

[34] N. Jiang, Z. Zhou, W. Xiong, J. Chen, J. Shen, R. Li, R. Ye, Tumor microenvironment triggered local oxygen generation and photosensitizer release from manganese dioxide mineralized albumin-ICG nanocomplex to amplify photodynamic immunotherapy efficacy, Chin. Chem. Lett. 32 (2021) 3948–3953.

[35] G. Zhu, G.M. Lynn, O. Jacobson, K. Chen, Y. Liu, H. Zhang, Y. Ma, F. Zhang, R. Tian, Q. Ni, S. Cheng, Z. Wang, N. Lu, B.C. Yung, Z. Wang, L. Lang, X. Fu, A. Jin, I.D. Weiss, H. Vishwasrao, G. Niu, H. Shroff, D.M. Klinman, R.A. Seder, X. Chen, Albumin/vaccine nanocomplexes that assemble in vivo for combination cancer immunotherapy, Nat. Commun. 8 (2017) 1954.

[36] R. Tian, S. Zhu, Q. Zeng, L. Lang, Y. Ma, D.O. Kiesewetter, Y. Liu, X. Fu, J. Lau, G. Zhu, O. Jacobson, Z. Wang, Y. Dai, G. Yu, B.R. Brooks, G. Liu, G. Niu, X. Chen, An albumin sandwich enhances in vivo circulation and stability of metabolically labile peptides, Bioconjug. Chem. 30 (2019) 1711–1723.

[37] K.D. Moynihan, R.L. Holden, N.K. Mehta, C. Wang, M.R. Karver, J. Dinter, S. Liang, W. Abraham, M.B. Melo, A.Q. Zhang, N. Li, S.L. Gall, B.L. Pentelute, D. J. Irvine, Enhancement of peptide vaccine immunogenicity by increasing lymphatic drainage and boosting serum stability, Cancer Immunol. Res. 6 (2018) 1025.

[38] D.M. Cummings, G.E. Larijani, D.P. Conner, R.K. Ferguson, M.L. Rocci, Characterization of dexamethasone binding in normal and uremic human serum, DICP 24 (1990) 229–231.

[39] E.A. Peets, M. Staub, S. Symchowicz, Plasma binding of betamethasone3H, dexamethasone-3H, and cortisol-14C— a comparative study, Biochem. Pharmacol. 18 (1969) 1655–1663.

[40] P.N. Naik, S.A. Chimatadar, S.T. Nandibewoor, Interaction between a potent corticosteroid drug – dexamethasone with bovine serum albumin and human serum albumin: a fluorescence quenching and fourier transformation infrared spectroscopy study, J. Photochem. Photobiol. B Biol. 100 (2010) 147–159.

[41] M. Kosuge, T. Takeuchi, I. Nakase, A.T. Jones, S. Futaki, Cellular internalization and distribution of arginine-rich peptides as a function of extracellular peptide concentration, serum, and plasma membrane associated proteoglycans, Bioconjug. Chem. 19 (2008) 656–664.

[42] A. Sivertsen, J. Isaksson, H.-K.S. Leiros, J. Svenson, J.-S. Svendsen, B. O. Brandsdal, Synthetic cationic antimicrobial peptides bind with their hydrophobic parts to drug site II of human serum albumin, BMC Struct. Biol. 14 (2014) 4.

[43] N. Kordalivand, E. Tondini, C.Y.J. Lau, T. Vermonden, E. Mastrobattista, W. E. Hennink, F. Ossendorp, C.F.V. Nostrum, Cationic synthetic long peptides-loaded nanogels: an efficient therapeutic vaccine formulation for induction of T-cell responses, J. Control. Release 315 (2019) 114–125.

[44] G.H.M. van Puijvelde, T. van Es, E.J.A. van Wanrooij, K.L.L. Habets, P. de Vos, R. van der Zee, W. van Eden, T.J.C. van Berkel, J. Kuiper, Induction of oral tolerance to HSP60 or an HSP60-peptide activates T cell regulation and reduces atherosclerosis, Arterioscler. Thromb. Vasc. Biol. 27 (2007) 2677–2683.

[45] G.N. Fredrikson, I. Söderberg, M. Lindholm, P. Dimayuga, K.-Y. Chyu, P.K. Shah, J. Nilsson, Inhibition of atherosclerosis in ApoE-null mice by immunization with ApoB-100 peptide sequences, Arterioscler. Thromb. Vasc. Biol. 23 (2003) 879–884.

[46] M. Skwarczynski, A.M. Dougall, M. Khoshnejad, S. Chandrudu, M.S. Pearson, A. Loukas, I. Toth, Peptide-based subunit vaccine against hookworm infection, PLoS One 7 (2012), e46870.

[47] D.C. Jackson, Y.F. Lau, T. Le, A. Suhrbier, G. Deliyannis, C. Cheers, C. Smith, W. Zeng, L.E. Brown, A totally synthetic vaccine of generic structure that targets toll-like receptor 2 on dendritic cells and promotes antibody or cytotoxic T cell responses, Proc. Natl. Acad. Sci. U. S. A. 101 (2004) 15440.

[48] M. Acedo, G. Tarrason, J. Piulats, M. Mann, M. Wilm, R. Eritja, Preparation of oligonucleotide-dexamethasone conjugates, Bioorg. Med. Chem. Lett. 5 (1995) 1577–1580.

[49] P. Kumthekar, S.-C. Tang, A.J. Brenner, S. Kesari, D.E. Piccioni, C. Anders, J. Carrillo, P. Chalasani, P. Kabos, S. Puhalla, K. Tkaczuk, A.A. Garcia, M. S. Ahluwalia, J.S. Wefel, N. Lakhani, N. Ibrahim, ANG1005, a brain-penetrating peptide–drug conjugate, shows activity in patients with breast cancer with leptomeningeal carcinomatosis and recurrent brain metastases, Clin. Cancer Res. 26 (2020) 2789.

[50] S.H. Nam, J. Jang, D.H. Cheon, S.-E. Chong, J.H. Ahn, S. Hyun, J. Yu, Y. Lee, pH-Activatable cell penetrating peptide dimers for potent delivery of anticancer drug to triple-negative breast cancer, J. Control. Release 330 (2021) 898–906.

[51] L.S. Dodda, I. Cabeza de Vaca, J. Tirado-Rives, W.L. Jorgensen, LigParGen web server: an automatic OPLS-AA parameter generator for organic ligands, Nucleic Acids Res. 45 (2017) W331–W336.

[52] M. Baek, F. DiMaio, I. Anishchenko, J. Dauparas, S. Ovchinnikov, G.R. Lee, J. Wang, Q. Cong, L.N. Kinch, R.D. Schaeffer, C. Millán, H. Park, C. Adams, C. R. Glassman, A. DeGiovanni, J.H. Pereira, A.V. Rodrigues, A.A. van Dijk, A. C. Ebrecht, D.J. Opperman, T. Sagmeister, C. Buhlheller, T. Pavkov-Keller, M. K. Rathinaswamy, U. Dalwadi, C.K. Yip, J.E. Burke, K.C. Garcia, N.V. Grishin, P. D. Adams, R.J. Read, D. Baker, Accurate prediction of protein structures and interactions using a three-track neural network, Science (2021) eabj8754.

[53] N. Hiranuma, H. Park, M. Baek, I. Anishchenko, J. Dauparas, D. Baker, Improved protein structure refinement guided by deep learning based accuracy estimation, Nat. Commun. 12 (2021) 1340.

[54] A. Lamiable, P. Thévenet, J. Rey, M. Vavrusa, P. Derreumaux, P. Tufféry, PEP-FOLD3: faster de novo structure prediction for linear peptides in solution and in complex, Nucleic Acids Res. 44 (2016) W449–W454.

[55] Y. Shen, J. Maupetit, P. Derreumaux, P. Tufféry, Improved PEP-FOLD approach for peptide and miniprotein structure prediction, J. Chem. Theory Comput. 10 (2014) 4745–4758.

[56] X. Periole, M. Cavalli, S.-J. Marrink, M.A. Ceruso, Combining an elastic network with a coarse-grained molecular force field: structure, dynamics, and intermolecular recognition, J. Chem. Theory Comput. 5 (2009) 2531–2543.

[57] P.C.T. Souza, S. Thallmair, P. Conflitti, C. Ramírez-Palacios, R. Alessandri, S. Raniolo, V. Limongelli, S.J. Marrink, Protein–ligand binding with the coarse-grained martini model, Nat. Commun. 11 (2020) 3714.

[58] P.C.T. Souza, R. Alessandri, J. Barnoud, S. Thallmair, I. Faustino, F. Grünewald, I. Patmanidis, H. Abdizadeh, B.M.H. Bruininks, T.A. Wassenaar, P.C. Kroon, J. Melcr, V. Nieto, V. Corradi, H.M. Khan, J. Domański, M. Javanainen, H. Martinez-Seara, N. Reuter, R.B. Best, I. Vattulainen, L. Monticelli, X. Periole, D. P. Tieleman, A.H. de Vries, S.J. Marrink, Martini 3: a general purpose force field for coarse-grained molecular dynamics, Nat. Methods 18 (2021) 382–388.

[59] C. Empereur-Mot, L. Pesce, G. Doni, D. Bochicchio, R. Capelli, C. Perego, G. M. Pavan, Swarm-CG: automatic parametrization of bonded terms in MARTINI-based coarse-grained models of simple to complex molecules via fuzzy self-tuning particle swarm optimization, ACS Omega 5 (2020) 32823–32843.

[60] F. Grünewald, R. Alessandri, P.C. Kroon, L. Monticelli, P.C.T. Souza, S.J. Marrink, Polyply; a python suite for facilitating simulations of macromolecules and nanomaterials, Nat. Commun. 13 (2022) 68.

[61] M.J. Abraham, T. Murtola, R. Schulz, S. Páll, J.C. Smith, B. Hess, E. Lindahl, GROMACS: high performance molecular simulations through multi-level parallelism from laptops to supercomputers, SoftwareX 1-2 (2015) 19–25.

[62] G. Bussi, D. Donadio, M. Parrinello, Canonical sampling through velocity rescaling, J. Chem. Phys. 126 (2007), 014101.

[63] H.J.C. Berendsen, J.P.M. Postma, W.F. van Gunsteren, A. DiNola, J.R. Haak, Molecular dynamics with coupling to an external bath, J. Chem. Phys. 81 (1984) 3684–3690.
[64] S. Kumar, J.M. Rosenberg, D. Bouzida, R.H. Swendsen, P.A. Kollman, THE weighted histogram analysis method for free-energy calculations on biomolecules. I. THE method, J. Comput. Chem. 13 (1992) 1011–1021.
[65] M. Souaille, B.T. Roux, Extension to the weighted histogram analysis method: combining umbrella sampling with free energy calculations, Comput. Phys. Commun. 135 (2001) 40–57.
[66] N.A. Baker, D. Sept, S. Joseph, M.J. Holst, J.A. McCammon, Electrostatics of nanosystems: application to microtubules and the ribosome, Proc. Natl. Acad. Sci. 98 (2001) 10037.
[67] T.J. Dolinsky, P. Czodrowski, H. Li, J.E. Nielsen, J.H. Jensen, G. Klebe, N. A. Baker, PDB2PQR: expanding and upgrading automated preparation of biomolecular structures for molecular simulations, Nucleic Acids Res. 35 (2007) W522–W525.
[68] W. Humphrey, A. Dalke, K. Schulten, VMD: visual molecular dynamics, J. Mol. Graph. 14 (1996) 33–38.
[69] H. Cox, P. Georgiades, H. Xu, T.A. Waigh, J.R. Lu, Self-assembly of mesoscopic peptide surfactant fibrils investigated by STORM super-resolution fluorescence microscopy, Biomacromolecules 18 (2017) 3481–3491.
[70] I.E. Allijn, B.M.S. Czarny, X. Wang, S.Y. Chong, M. Weiler, A.E. da Silva, J. M. Metselaar, C.S.P. Lam, G. Pastorin, D.P.V. de Kleijn, G. Storm, J.-W. Wang, R. M. Schiffelers, Liposome encapsulated berberine treatment attenuates cardiac dysfunction after myocardial infarction, J. Control. Release 247 (2017) 127–133.
[71] Z. Liu, Y. Gu, A. Shin, S. Zhang, F. Ginhoux, Analysis of myeloid cells in mouse tissues with flow cytometry, STAR Protocols 1 (2020), 100029.
[72] S.Y. Chong, O. Zharkova, S.M.J.M. Yatim, X. Wang, X.C. Lim, C. Huang, C.Y. Tan, J. Jiang, L. Ye, M.S. Tan, V. Angeli, H.H. Versteeg, M. Dewerchin, P. Carmeliet, C. S.P. Lam, M.Y. Chan, D.P.V. de Kleijn, J.-W. Wang, Tissue factor cytoplasmic domain exacerbates post-infarct left ventricular remodeling via orchestrating cardiac inflammation and angiogenesis, Theranostics 11 (2021) 9243–9261.
[73] Y. Wen, A. Waltman, H. Han, J.H. Collier, Switching the immunogenicity of peptide assemblies using surface properties, ACS Nano 10 (2016) 9274–9286.
[74] C.Y.J. Lau, N. Benne, B. Lou, D.T. Braake, E. Bosman, N. van Kronenburg, M. Fens, F. Broere, W.E. Hennink, E. Mastrobattista, Tuning surface charges of peptide nanofibers for induction of antigen-specific immune tolerance: an introductory study, J. Pharm. Sci. 111 (4) (2022) 1004–1011.
[75] M.E. Baker, Albumin, steroid hormones and the origin of vertebrates, J. Endocrinol. 175 (2002) 121–127.
[76] A.M. Fernandez-Escamilla, F. Rousseau, J. Schymkowitz, L. Serrano, Prediction of sequence-dependent and mutational effects on the aggregation of peptides and proteins, Nat. Biotechnol. 22 (2004) 1302–1306.
[77] J.S. Rudra, Y.F. Tian, J.P. Jung, J.H. Collier, A self-assembling peptide acting as an immune adjuvant, Proc. Natl. Acad. Sci. U. S. A. 107 (2010) 622–627.
[78] G. De Baets, J. Van Durme, F. Rousseau, J. Schymkowitz, A genome-wide sequence-structure analysis suggests aggregation gatekeepers constitute an evolutionary constrained functional class, J. Mol. Biol. 426 (2014) 2405–2412.
[79] X.M. He, D.C. Carter, Atomic structure and chemistry of human serum albumin, Nature 358 (1992) 209–215.
[80] J. Nilsen, M. Bern, K.M.K. Sand, A. Grevys, B. Dalhus, I. Sandlie, J.T. Andersen, Human and mouse albumin bind their respective neonatal fc receptors differently, Sci. Rep. 8 (2018) 14648.
[81] E. Crusca Jr., A.A. Rezende, R. Marchetto, M.J.S. Mendes-Giannini, W. Fontes, M. S. Castro, E.M. Cilli, Influence of N-terminus modifications on the biological activity, membrane interaction, and secondary structure of the antimicrobial peptide hylin-a1, Pept. Sci. 96 (2011) 41–48.
[82] F. Grünewald, P.C. Kroon, P.C.T. Souza, S.J. Marrink, Protocol for simulations of PEGylated proteins with martini 3, in: Y.W. Chen, C.-P.B. Yiu (Eds.), Structural Genomics: General Applications, Springer, US, New York, NY, 2021, pp. 315–335.
[83] L. Yang, G. Song, L. Jernigan Robert, Protein elastic network models and the ranges of cooperativity, Proc. Natl. Acad. Sci. 106 (2009) 12347–12352.
[84] M. Amaral, D.B. Kokh, J. Bomke, A. Wegener, H.P. Buchstaller, H. M. Eggenweiler, P. Matias, C. Sirrenberg, R.C. Wade, M. Frech, Protein conformational flexibility modulates kinetics and thermodynamics of drug binding, Nat. Commun. 8 (2017) 2276.
[85] D. Eisenberg, E. Schwarz, M. Komaromy, R. Wall, Analysis of membrane and surface protein sequences with the hydrophobic moment plot, J. Mol. Biol. 179 (1984) 125–142.
[86] A.J. Patel, P. Varilly, S.N. Jamadagni, M.F. Hagan, D. Chandler, S. Garde, Sitting at the edge: how biomolecules use hydrophobicity to tune their interactions and function, J. Phys. Chem. B 116 (2012) 2498–2503.
[87] G. Rutili, K.-E. Arfors, Protein concentration in interstitial and lymphatic fluids from the subcutaneous tissue, Acta Physiol. Scand. 99 (1977) 1–8.
[88] T.C.T. Michaels, A. Šarić, S. Curk, K. Bernfur, P. Arosio, G. Meisl, A.J. Dear, S.I. A. Cohen, C.M. Dobson, M. Vendruscolo, S. Linse, T.P.J. Knowles, Dynamics of oligomer populations formed during the aggregation of Alzheimer's Aβ42 peptide, Nat. Chem. 12 (2020) 445–451.
[89] K. Katneni, S.A. Charman, C.J.H. Porter, Use of plasma proteins as solubilizing agents in in vitro permeability experiments: correction for unbound drug concentration using the reciprocal permeability approach, J. Pharm. Sci. 97 (2008) 209–224.
[90] A. Zorzi, S.J. Middendorp, J. Wilbs, K. Deyle, C. Heinis, Acylated heptapeptide binds albumin with high affinity and application as tag furnishes long-acting peptides, Nat. Commun. 8 (2017) 16092.
[91] R.W. Kalicharan, M.R. Bout, C. Oussoren, H. Vromans, Where does hydrolysis of nandrolone decanoate occur in the human body after release from an oil depot? Int. J. Pharm. 515 (2016) 721–728.
[92] R.W. Kalicharan, C. Oussoren, P. Schot, E. de Rijk, H. Vromans, The contribution of the in-vivo fate of an oil depot to drug absorption, Int. J. Pharm. 528 (2017) 595–601.
[93] M. Pyzik, T. Rath, T.T. Kuo, S. Win, K. Baker, J.J. Hubbard, R. Grenha, A. Gandhi, T.D. Krämer, A.R. Mezo, Z.S. Taylor, K. McDonnell, V. Nienaber, J.T. Andersen, A. Mizoguchi, L. Blumberg, S. Purohit, S.D. Jones, G. Christianson, W.I. Lencer, I. Sandlie, N. Kaplowitz, D.C. Roopenian, R.S. Blumberg, Hepatic FcRn regulates albumin homeostasis and susceptibility to liver injury, Proc. Natl. Acad. Sci. 114 (2017) E2862.
[94] M.J. Barnden, J. Allison, W.R. Heath, F.R. Carbone, Defective TCR expression in transgenic mice constructed using cDNA-based α- and β-chain genes under the control of heterologous regulatory elements, Immunol. Cell Biol. 76 (1998) 34–40.
[95] S.M. Lewis, A. Williams, S.C. Eisenbarth, Structure and function of the immune system in the spleen, Sci. Immunol. 4 (2019), eaau6085.
[96] X. Chen, J.J. Oppenheim, R.T. Winkler-Pickett, J.R. Ortaldo, O.M.Z. Howard, Glucocorticoid amplifies IL-2-dependent expansion of functional FoxP3+CD4+ CD25+ T regulatory cells in vivo and enhances their capacity to suppress EAE, Eur. J. Immunol. 36 (2006) 2139–2149.
[97] X. Chen, T. Murakami, J.J. Oppenheim, O.M.Z. Howard, Differential response of murine CD4+CD25+ and CD4+CD25– T cells to dexamethasone-induced cell death, Eur. J. Immunol. 34 (2004) 859–869.
[98] G. Kwak, H. Kim, J. Park, E.H. Kim, H. Jang, G. Han, S.Y. Wang, Y. Yang, I. Chan Kwon, S.H. Kim, A Trojan-horse strategy by in situ piggybacking onto endogenous albumin for tumor-specific neutralization of oncogenic MicroRNA, ACS Nano 15 (2021) 11369–11384.
[99] P. Agarwal, C.R. Bertozzi, Site-specific antibody–drug conjugates: the nexus of bioorthogonal chemistry, protein engineering, and drug development, Bioconjug. Chem. 26 (2015) 176–192.
[100] M. Rieckmann, M. Delgobo, C. Gaal, L. Büchner, P. Steinau, D. Reshef, C. Gil-Cruz, E.N.T. Horst, M. Kircher, T. Reiter, K.G. Heinze, H.W.M. Niessen, P.A. J. Krijnen, A.M. van der Laan, J.J. Piek, C. Koch, H.-J. Wester, C. Lapa, W. R. Bauer, B. Ludewig, N. Friedman, S. Frantz, U. Hofmann, G.C. Ramos, Myocardial infarction triggers cardioprotective antigen-specific T helper cell responses, J. Clin. Invest. 129 (2019) 4922–4936.